

Selection of smooth motion profile for a tube locator module of an inspection device

G. Perumalsamy¹, P. Visweswaran², Deepak Kumar², S. Joseph Winston², S. Murugan¹

¹Homi Bhabha National Institute (HBNI)-Mumbai, Kalpakkam Centre, Tamilnadu, India

²Reactor Design and Technology Group, Indira Gandhi Centre for Atomic Research, Kalpakkam, India

Article Info

Article history:

Received Jul 19, 2021

Revised Jun 2, 2022

Accepted Jun 21, 2022

Keywords:

Cycloidal motion

Harmonic jerk s-curve

Jerk-limited s-curve

Joint trajectory

Quintic polynomial

Residual vibration

Steam generator inspection

ABSTRACT

The Prototype Fast Breeder Reactor steam generators inspection system has seven modules. In this, tube locator module is a planar serial two-link robotic arm, which is used to place the eddy current probe above the steam generators tube hole in the tube sheet region. The trajectory planning of the two-link robotic arm is one of the important tasks, so the peak velocity, peak acceleration, peak jerk of various motion profiles for a given distance has to be selected properly for smooth motion and to avoid actuator saturation. The fifth-order polynomial gives lower acceleration and velocity than the jerk-limited S-curve. In this paper, the comparison of peak values of kinematic variables (velocity, acceleration, and jerk) for different motion profiles has been presented.

This is an open access article under the [CC BY-SA](https://creativecommons.org/licenses/by-sa/4.0/) license.



Corresponding Author:

G. Perumalsamy

Homi Bhabha National Institute (HBNI)-Mumbai, Kalpakkam Centre

Tamilnadu, India

Email: perumalsamy2012mdes@gmail.com

1. INTRODUCTION

The Prototype Fast Breeder Reactor (PFBR) is a 500 MW capacity sodium cooled fast breeder reactor under commissioning in Kalpakkam, India. The steam generator (SG) of PFBR is a counter flow shell and tube heat exchanger with sodium on shell side and water/steam on the tube side. The SG contains 547 tubes of 17.2 mm OD, 25 m length and thickness of 2.3 mm. The wall thickness of the tube is the only barrier between the liquid sodium and the water in the SG. Periodic in-service inspection of the SG tubes is mandated to mitigate the failure of the SG tubes. The in-service inspection of the SG tubes is carried out using the indigenously developed PFBR SG inspection system (PSGIS) device. The structural integrity of the SG tubes is evaluated using the remote field eddy current testing technique. The PSGIS device consists of several modules such as the device deployment module, tube locator module (TLM), and cable pusher module. The primary task of the inspection device is to orient the cable pusher module above the user defined SG tube for the deployment and retrieval of the eddy current probe at uniform speed along the tube length. The TLM of the PSGIS device is a two-arm serial robotic device. It has two rotational degrees of freedom which enable it to position the end-effector of the robotic arm above anyone of the 547 tubes as shown in Figure 1. The actual prototype of two-link robotic arm is shown in Figure 2.

Forward kinematics determines the end-effector position corresponding to joint angle. Figure 3 represents the schematic of two-link robotic arm. The position of two-axis robotic arm (x, y) is represented by (1) and (2).

$$x = l_1 \cos(\theta_1) + l_2 \cos(\theta_1 + \theta_2) \quad (1)$$

$$y = l_1 \sin(\theta_1) + l_2 \sin(\theta_1 + \theta_2) \quad (2)$$

where x and y are end-effector position coordinates, l_1 is the length of link1, l_2 is the length of link2, and θ_1 and θ_2 are joint angle of link1 and link2, respectively.

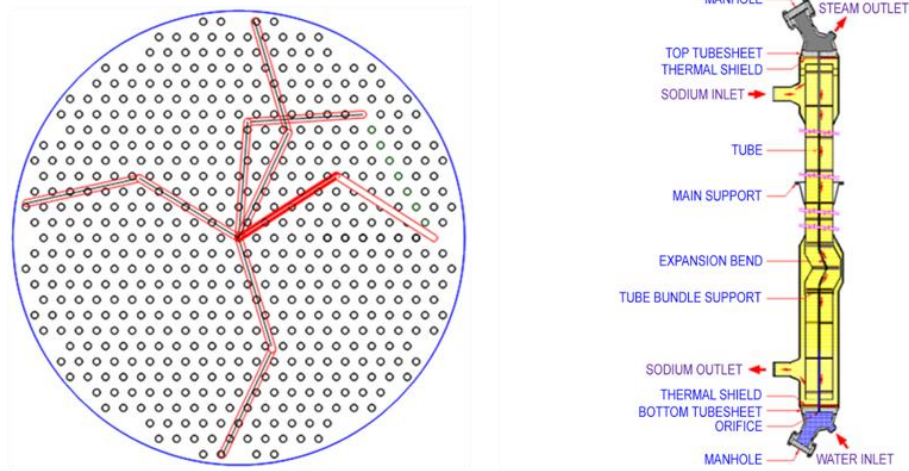


Figure 1. SG tube sheet and steam generator

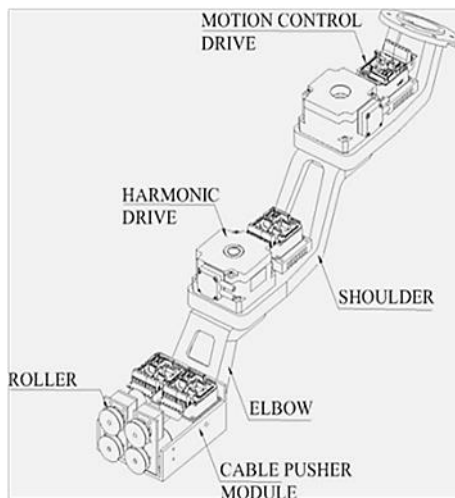


Figure 2. Prototype of two-link robotic arm

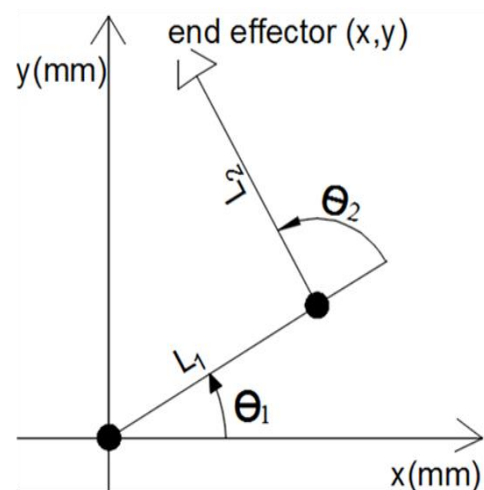


Figure 3. Schematic of two-link robotic arm [1]

TLM uses harmonic drive FHA-C miniseries (gear ratio=50) servo actuators with incremental line driver encoder (2000 ppr). Table 1 shows the two-link robotic arm geometric and mass parameter. Inverse kinematics establishes the relation between the joint angle and end-effector position. There are many methods to find out joint angles such as analytical, geometric, and iterative techniques. The inverse kinematic algorithm of two-link robotic arm is shown in Figure 4.

Table 1. Two-link robotic arm geometric parameter

Parameters	Value	Parameters	Value
Mass of the Elbow arm motor(m_3)	0.5 kg	Elbow Arm Moment of Inertia about CG (I_{z2})	$3.675 \times 10^{-3} \text{ kgm}^2$
Mass of the Elbow arm (m_2)	1.0 kg	Length of shoulder arm (l_1)	0.21 m
Mass of the Shoulder Arm (m_1)	1.0 kg	Length of Elbow arm (l_2)	0.21 m
Shoulder Arm Moment of Inertia about CG(I_{z1})	$3.675 \times 10^{-3} \text{ kgm}^2$	Mass of the point load at end-effector end(m_4)	1 kg

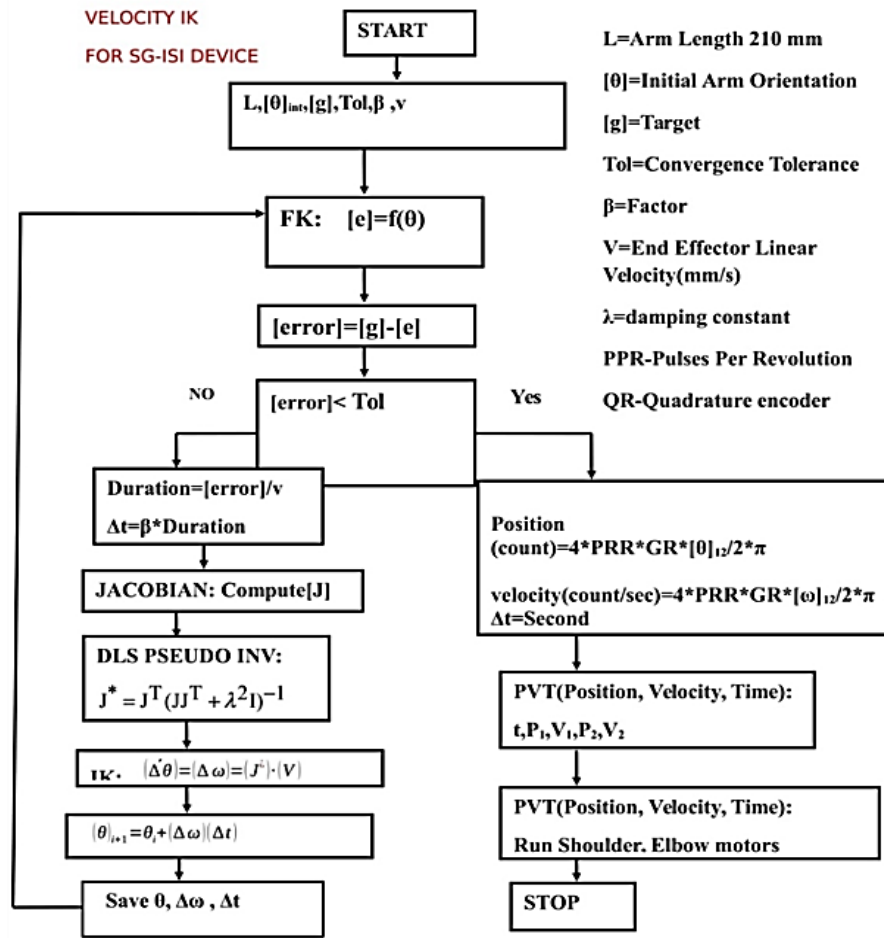


Figure 4. Inverse kinematics algorithm of SG-ISI

In TLM, damped least square inverse kinematics is used to find out joint velocity as given by (3),

$$\dot{\theta} = J^T [JJ^T + \lambda^2 I]^{-1} [V] \quad (3)$$

where λ is damping factor, V is end-effector velocity, $\dot{\theta}$ - joint velocity of two-link robotic arm, and J represents the Jacobian of the two-link robotic arm which is given by (4).

$$J = \begin{bmatrix} -l_1 \sin(\theta_1) - l_2 \sin(\theta_1 + \theta_2) & -l_2 \sin(\theta_1 + \theta_2) \\ l_1 \cos(\theta_1) + l_2 \cos(\theta_1 + \theta_2) & l_2 \cos(\theta_1 + \theta_2) \end{bmatrix} \quad (4)$$

The positioning accuracy required for the TLM is of the order of 0.1 mm. Moreover, in a serial manipulator like TLM, achieving accuracy of the order of 0.1 mm is a challenging task. The positioning accuracy is affected by residual vibration of the robotic arm. Hence, selection of smooth motion profile plays a vital role in achieving the 0.1 mm accuracy. The smooth motion profile is generated in many ways by different functions and different methods.

Motion planning in robotics is a growing research field in the industry. Robotic motion is classified into two types, namely point-to-point and motion through sequence of points. Motion planning is done in joint space/end-effector coordinates. The end-effector coordinates, and joint coordinates are related by nonlinear functions, so planning of joint motion profile plays an important role in end-effector motion planning. In literature, several methods are proposed for the generation of smooth trajectory namely polynomial, spline, dynamic movement primitives, digital convolution, and finite impulse response filter-based methods. It is seen from the literature that Ezair *et al.* [2] and Kirecci and Gilmartin [3] investigated motion planning from a computational point of view. The methods favorable for reducing the computation load are i) root multiplicity method, ii) recursive method, and iii) convolution method.

Ezair *et al.* [2] enumerated a recursive method to reduce higher-order polynomial to lower-order polynomial. It can produce a smooth trajectory using arbitrary initial and final conditions. Kirecci and Gilmartin [3] synthesized the joint angle motion planning using arbitrary power polynomial. The arbitrary power polynomial produces lower peak velocity than the other motion profile. Moreover, Boryga and Grabos [4] proposed root multiplicity method to form higher order polynomial. The higher-order polynomial produces oscillation. In addition, previous studies showed that higher-order polynomials introduce computational complexity. To avoid this, a piecewise polynomial (spline) is used to interpolate the joint angle [5]. Even though piecewise polynomial (spline) is used to join the number of via points for smooth motion, the acceleration of cubic spline is not smooth. Furthermore, truncated trigonometric series is used to interpolate the joint angle [6]. Moreover, motion planning is discussed from the point of minimum jerk [7]–[9], minimum time [10]–[12], minimum energy [13], [14], and minimum torque [15].

Jerk-limited motion is generated by polynomial, trigonometric and sigmoid function. M. S. Muftaba [16] stated that bang-bang (quadratic polynomial) motion produces infinite jerk which produces lots of vibration which leads to tracking error. In addition, jerk-limited motion is generated by S-curve profile. S-curve motion profile has seven phases. Depending on the motion distance, initial and final boundary conditions, S-curve may not have constant velocity and constant acceleration phases. Nguyen *et al.* [17] proposed a recursive method to form S-curve motion profile using polynomial and trigonometric. They stated that position error decreases when higher-order polynomial S-curve is used. Further, an increase of polynomial degree increases the number of segments by $2^n - 1$. The jerk-limited motion profile increases the motion time than cubic polynomial.

At the beginning of the 19th century, only first-order continuity (velocity) is achieved in motion planning. At the end of the 19th century, second-order continuity (acceleration) is achieved. In the 20th century, third-order continuity (jerk) has been a main concern in the motion profile. Moreover, jerk-bounded motion produces symmetric and asymmetric motion profiles due to the bounded value of jerk in acceleration and deceleration phases. The design of acceleration and deceleration profile plays a vital role in improving precision and accuracy. Moreover, duration of acceleration and deceleration play a significant role in reducing the settling time and residual vibration. The settling time is reduced by asymmetric motion and lower magnitude of jerk. The conventional method cannot produce an asymmetric velocity profile. Different magnitudes of jerk in acceleration and deceleration can produce an asymmetric profile. Li [18] proposed an asymmetric motion profile using a sine jerk profile which reduces residual vibration. The vibration produced by the sinusoidal jerk profile is lesser than the trapezoidal and jerk-limited s-curve motion profile. Rew and Kim [19] enumerated closed-form solution to asymmetric motion using a seven-segment approach to reduce settling time and residual vibration. Amthor *et al.* [20] proposed an asymmetric motion profile using fourth-order polynomial. Perumal and Jawahar [21] proposed a synchronized trigonometric S-curve for jerk reduction. Moreover, sigmoid (piecewise exponential) is also used for smooth motion [22], [23].

The motion profile with higher-order continuity increases computational complexity but motion time is more complex, and it needs precise hypothesis. Snap bounded trajectory planning reduces the amplitudes of vibration than the jerk-limited motion profile. Rocha *et al.* [24] proposed an embedded system-based snap constrained trajectory planning method for 3D motion systems. They compared snap constrained trajectory planning with seven segments and trapezoidal acceleration motion profile.

Even though piecewise polynomial (algebraic spline) is used to plan the joint motion, it is not suitable for operations such as obstacle avoidance. Moreover, drawback of algebraic spline is that computational complexity increases due to coupled nature of unknowns. To reduce the coupling, Simon *et al.* [25] introduced a trigonometric spline to interpolate data points. Further, Visioli [26] compared the algebraic and trigonometric splines to reduce the overshoot of the motion profile. Nnaji and Asano [27] investigated five joint trajectory profiles such as bang-bang, polynomial, exponential, cosine, and sine ramp profile. They investigated joint motion based on total work done, individual peak joint torque, and individual peak joint power. They stated that the evaluation process is independent of joint profile or specific robot. They stated that exponential trajectory was the best path out of the five trajectories. Polynomial trajectory is robot specific but exponential trajectory is not robot specific. The exponential profile is more suitable for large distance motion than the shorter motion. The acceleration produced by the exponential motion profile at the starting and ending is finite which results in tracking error.

On contrary to off-line programming, online motion planning needs fewer data points. Moreover, online motion planning plays a vital role in avoiding obstacles. The finite impulse response filter is used to generate multi-segment motion profile in online motion planning [28]. Chand and Doty [29] proposed a cubic spline online joint trajectory. The average path error produced by the cubic spline is lower than the linear spline joint trajectory. Bazaz and Tondur [30] proposed a three-cubic method for motion generation between two successive points. Sidobre and Desormeaux [31] proposed a smooth cubic polynomial for human-robot

interactions. In robotics motion control, shorter movements possess complex behavior. They analyzed the influence of velocity on the shorter motion.

From the literature, it was found that no generalized study was carried out for smooth motion profile with kinematic constraints. In this paper, generalized study of bang-bang, jerk-limited s-curve, fifth order polynomial (quintic polynomial), and cycloid motion profile is presented. The paper is organized as follows. Section 1 gives a brief review of forward, inverse kinematics of two link robotic arm and state of the art in motion planning. Section 2 gives a brief overview of the smooth motion profiles. Section 3 gives analytical methods to compute peak velocity, acceleration, and jerk. Section 4 discusses case study. Section 5 summarizes the results of this paper.

2. SELECTION OF SMOOTH MOTION PROFILE FOR STEAM GENERATOR INSPECTION

Smooth motion is obtained in many ways. Smooth motion is generated by with or without considering kinematic and dynamic constraints. The kinematic constraints are joint actuator velocity, acceleration, and jerk. The dynamic constraints are joint actuator torque and torque rate. Further, minimum time is handled by kinematic and dynamic constraints, respectively. The bang-bang motion profile achieves time-optimal motion, but it results in jerky motion due to impulse load (infinite jerk) at finite points as shown in Figure 5(a), which causes tracking error and vibration. However, the jerky motion is smoothed by linear acceleration and deceleration (trapezoidal acceleration and deceleration) which increases motion time as shown in Figure 5(b). Even though jerk-limited motion produces finite jerks, it does not have continuous jerks as shown in Figure 5(c). This can be further improved by including higher-order continuity namely derivative of jerk (snap), derivative of snap (jounce or crackle), and which makes the jerk continuous. The motion profile with higher-order continuity results in computational complexity which needs proper hypothesis for selecting motion time. The higher-order polynomial motion produces smaller jerks. The trade-off has to be made such that motion profile satisfies computational complexity and bounded jerk. In multi-segment motion planning, the movement from one segment to another segment needs smooth transition (preferably c^3 continuity) to avoid impulse load (impulse force or torque). The piecewise polynomial is used to join the segment smoothly. The formulation of various motion profiles is given in the methodology section.

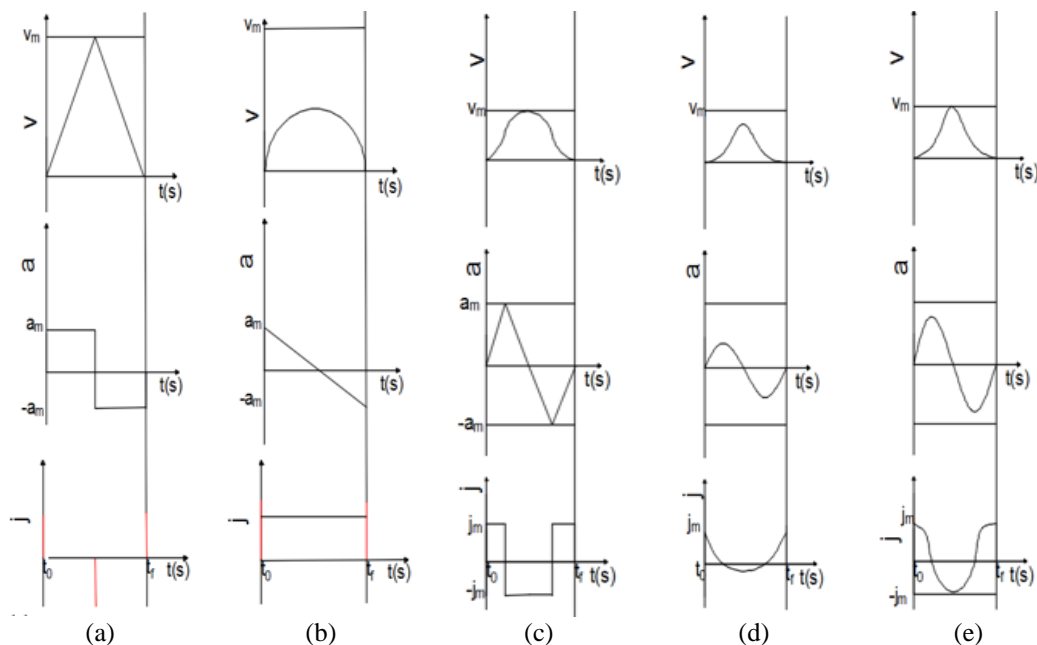


Figure 5. Position, velocity, acceleration, and jerk of various motion profiles: (a) bang-bang, (b) cubic polynomial, (c) jerk-limited s curve, (d) fifth-order polynomial, and (e) cycloid motion

3. METHODOLOGY

In this section, the end-effector peak velocity, peak acceleration and peak jerk of various motion profiles are derived and compared for the given motion time (t) and total displacement (Δs).

3.1. Quintic polynomial

Polynomial is used for motion planning of joint angle due to less computation. Even though linear polynomials have position continuity, they do not have velocity, acceleration continuity. On the other hand, cubic polynomial has position and velocity continuity. However, the acceleration produces discontinuity at the starting and ending in cubic polynomial. The fifth-order polynomial (Figure 5(d)) has position, velocity, and acceleration continuity. Moreover, jerk produced by the cubic polynomial is constant, but fifth-order polynomial produces non-linear jerk. The position (s), velocity (v), acceleration (a), jerk (j), and snap of fifth order polynomial is given by (5),

$$\begin{aligned} s(t) &= a_0 + a_1t + a_2t^2 + a_3t^3 + a_4t^4 + a_5t^5 \\ v(t) &= a_1 + 2a_2t + 3a_3t^2 + 4a_4t^3 + 5a_5t^4 \\ a(t) &= 2a_2 + 6a_3t + 12a_4t^2 + 20a_5t^3 \\ j(t) &= 6a_3 + 24a_4t + 60a_5t^2 \\ j(t) &= 24a_4 + 120a_5t \end{aligned} \quad (5)$$

where $a_0, a_1, a_2, a_3, a_4, a_5$ are unknowns and t -time.

The fifth-order polynomial has six unknowns. The six unknowns are determined by applying the initial and final boundary conditions. The initial and final boundary conditions are given by (6).

$$\begin{aligned} s(t=0) &= s_i & v(t=0) &= 0 & a(t=0) &= 0 \\ s(t=t_f) &= s_f & v(t=t_f) &= 0 & a(t=t_f) &= 0 \end{aligned} \quad (6)$$

The position at time t is given by (7)

$$s(t) = \left[\left(\frac{10}{t_f^3} \right) t^3 - \left(\frac{15}{t_f^4} \right) t^4 + \left(\frac{6}{t_f^5} \right) t^5 \right] (s_f - s_i) \quad (7)$$

The jerk of fifth-order polynomial is given by (8)

$$j(t) = \left[\left(\frac{60}{t_f^3} \right) - \left(\frac{360}{t_f^4} \right) t + \left(\frac{360}{t_f^5} \right) t^2 \right] (s_f - s_i) \quad (8)$$

The maximum velocity occurs when acceleration is zero ($t=t_f/2$). The maximum velocity (v_m) of fifth-order polynomial is given by (9a) and (9b)

$$v_m = \left(\frac{15}{8} \right) \left(\frac{\Delta s}{t_f} \right) \quad (9a)$$

where $\Delta s = s_f - s_i$

$$v_m = 0.4789(\Delta s^2 j_m)^{(1/3)} \quad (9b)$$

where v_m is the maximum velocity, t_f is the motion time, Δs is the total distance, and j_m is the maximum jerk. The maximum value of jerk occurs at $t=0$ and $t=t_f$. The given distance (Δs) and velocity (v_m), the maximum jerk (j_m) is calculated by (10)

$$j_m = \frac{v_m^3}{(\Delta s)^2 (0.4789)^3} \quad (10)$$

where j_m is the maximum jerk, V_m is the maximum velocity, and Δs is the total distance
The optimal time for fifth-order polynomial is given by (11)

$$t_f = 3.9149 \left(\frac{\Delta s}{j_m} \right)^{(1/3)} \quad (11)$$

The maximum acceleration (a_m) of fifth-order polynomial is given by (12)

$$a_m = 0.3767(\Delta s j_m^2)^{(1/3)} \quad (12)$$

3.2. Jerk-limited S-curve (without constant acceleration and constant velocity phase)

The cubic polynomial produces linear acceleration, but this introduces finite jerks at the starting and ending. Even though the jerk-limited motion profile has some finite value at the starting and ending in jerk, it has zero acceleration at endpoints. Depending on the distance and kinematic constraints (maximum acceleration and maximum velocity), some phases (constant acceleration or constant velocity) may not exist. For ease of computational complexity, only constant jerk phase is considered. The constant acceleration and constant velocity phase are not considered. It can be seen that the minimum number of segments for achieving minimum time is 3 for satisfying only jerk constraints without utilizing the maximum acceleration and velocity.

The jerk (j) at time t is given by (13),

$$j(t) = \begin{cases} j_m & 0 < t \leq t_j \\ -j_m & t_j < t \leq 3t_j \\ j_m & 3t_j < t \leq 4t_j \end{cases} \quad (13)$$

where t_j -time duration for jerk phase, j_m - maximum jerk. The position of jerk-limited motion profile is given by (14a).

$$s(t) = \begin{cases} j_m \left(\frac{t^3}{6} \right) & 0 < t \leq t_j \\ j_m t_j \left(\frac{t^2}{2} \right) - j_m \left(\frac{t^3}{6} \right) + j_m \left(\frac{t_j^2}{2} \right) t + j_m \left(\frac{t_j^3}{6} \right) & t_j < t \leq 3t_j \\ j_m \left(\frac{t^3}{6} \right) - j_m t_j \left(\frac{t^2}{2} \right) + j_m \left(\frac{t_j^2}{2} \right) t + \left(\frac{11}{6} \right) j_m t_j^3 & 3t_j < t \leq 4t_j \end{cases} \quad (14a)$$

The velocity of jerk-limited motion profile is given by (14b).

$$v(t) = \begin{cases} j_m \left(\frac{t^2}{2} \right) & 0 < t \leq t_j \\ j_m t_j t - j_m \left(\frac{t^2}{2} \right) + j_m \left(\frac{t_j^2}{2} \right) & t_j < t \leq 3t_j \\ j_m \left(\frac{t^2}{2} \right) - j_m t_j t + j_m \left(\frac{t_j^2}{2} \right) & 3t_j < t \leq 4t_j \end{cases} \quad (14b)$$

The acceleration of jerk-limited motion profile is given by (14c).

$$a(t) = \begin{cases} j_m t & 0 < t \leq t_j \\ j_m t_j - j_m t & t_j < t \leq 3t_j \\ j_m & 3t_j < t \leq 4t_j \end{cases} \quad (14c)$$

The time duration for jerk phase along x, y-direction (t_x, t_y) is given by (15).

$$t_x = \left[\frac{\Delta x}{2j_m} \right]^{(1/3)} \quad t_y = \left[\frac{\Delta y}{2j_m} \right]^{(1/3)} \quad (15)$$

From the maximum velocity, the maximum jerk is calculated. From the maximum jerk (j_m) and distance, motion time is calculated. The time for the jerk phase is given by (16a).

$$t_j = 0.7937 \left(\frac{\Delta s}{j_m} \right)^{(1/3)} \quad (16a)$$

The total time for jerk-limited motion profile is given by (16c).

$$t_j = 4t_j$$

$$t_j = 3.1748 \left(\frac{\Delta s}{j_m} \right)^{(1/3)} \quad (16b)$$

$$t_0 = \max(t_x, t_y) \quad (16c)$$

3.3. Cycloid motion

The fifth-order polynomial and jerk-limited motion are formed by polynomial, whereas cycloid motion (Figure 5(e)) is constructed by point p on the circle rolls along a straight line as shown in Figure 6. The cycloid motion cannot be used for motion planning of multiple segments, due to finite jerk in the intermediate points, start and endpoints. The cycloid motion has linear polynomial and trigonometric function.

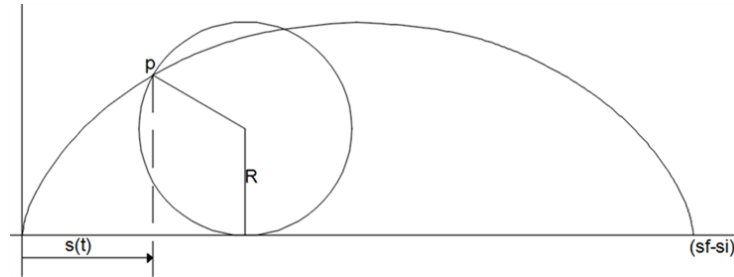


Figure 6. Generation of cycloid motion

The position of cycloid motion profile as shown in Figure 6 is given by (17) .

$$s(t) = \Delta s \left\{ \left(\frac{t}{t_f} \right) - \left(\frac{1}{2\pi} \right) \sin \left(\frac{2\pi t}{t_f} \right) \right\} + s_i \quad (17)$$

The velocity, acceleration and jerk are given by(18-20).

$$v(t) = \left(\frac{\Delta s}{t_f} \right) \left\{ 1 - \cos \left(\frac{2\pi t}{t_f} \right) \right\} \quad (18)$$

$$a(t) = \left(\frac{2\pi \Delta s}{t_f^2} \right) \left\{ \sin \left(\frac{2\pi t}{t_f} \right) \right\} \quad (19)$$

$$j(t) = \left(\frac{4\pi^2 \Delta s}{t_f^3} \right) \left\{ \cos \left(\frac{2\pi t}{t_f} \right) \right\} \quad (20)$$

where Δs is the total displacement, t_f is the total motion time. The acceleration profile of cycloid motion is smoother than the jerk-limited motion profile. The peak acceleration of cycloid motion is larger than the fifth-order polynomial.

3.4. Harmonic jerk S-curve

The harmonic jerk S-curve is given by (21).

$$j(t) = \begin{cases} j_m \left(1 - \cos \left(\frac{2\pi \cdot t}{t_j} \right) \right) & 0 < t \leq t_j \\ -j_m \left(1 - \cos \left(\frac{2\pi \cdot t}{t_j} \right) \right) & t_j < t \leq 2t_j \\ -j_m \left(1 - \cos \left(\frac{2\pi \cdot t}{t_j} \right) \right) & 2t_j < t \leq 3t_j \\ j_m \left(1 - \cos \left(\frac{2\pi \cdot t}{t_j} \right) \right) & 3t_j < t \leq 4t_j \end{cases} \quad (21)$$

The acceleration of harmonic jerk S-curve is given by (22).

$$a(t) = \begin{cases} 0.5 * j_m \left\{ t - \frac{\sin\left(\frac{2\pi t}{t_j}\right)}{\left(\frac{2\pi}{t_j}\right)} \right\} & 0 < t \leq t_j \\ -0.5 * j_m \left\{ t - \frac{\sin\left(\frac{2\pi t}{t_j}\right)}{\left(\frac{2\pi}{t_j}\right)} \right\} + 0.5 * j_m * t_j & t_j < t \leq 2t_j \\ -0.5 * j_m \left\{ t - \frac{\sin\left(\frac{2\pi t}{t_j}\right)}{\left(\frac{2\pi}{t_j}\right)} \right\} & 2t_j < t \leq 3t_j \\ 0.5 * j_m \left\{ t - \frac{\sin\left(\frac{2\pi t}{t_j}\right)}{\left(\frac{2\pi}{t_j}\right)} \right\} - 0.5 * j_m * t_j & 3t_j < t \leq 4t_j \end{cases} \quad (22)$$

The velocity of harmonic jerk S-curve is given by (23)

$$v(t) = \begin{cases} 0.5 * j_m \left\{ \frac{t^2}{2} + \frac{\cos\left(\frac{2\pi t}{t_j}\right)}{\left(\frac{2\pi}{t_j}\right)^2} \right\} & 0 < t \leq t_j \\ -0.5 * j_m \left\{ \frac{t^2}{2} + \frac{\cos\left(\frac{2\pi t}{t_j}\right)}{\left(\frac{2\pi}{t_j}\right)^2} \right\} + j_m * 0.5 * t_j t + j_m * 0.25 * t_j^2 + j_m * 0.5 * \left(\frac{t_j}{2\pi}\right)^2 & t_j < t \leq 2t_j \\ -0.5 * j_m \left\{ \frac{t^2}{2} + \frac{\cos\left(\frac{2\pi t}{t_j}\right)}{\left(\frac{2\pi}{t_j}\right)^2} \right\} + j_m * 0.5 * t_j^2 + j_m * 0.5 * \left(\frac{t_j}{2\pi}\right)^2 & 2t_j < t \leq 3t_j \\ 0.5 * j_m \left\{ \frac{t^2}{2} + \frac{\cos\left(\frac{2\pi t}{t_j}\right)}{\left(\frac{2\pi}{t_j}\right)^2} \right\} + j_m * 0.25 * t_j^2 - j_m * 0.5 * \left(\frac{t_j}{2\pi}\right)^2 - j_m * 0.5 * t_j t & 3t_j < t \leq 4t_j \end{cases} \quad (23)$$

The position of harmonic jerk S-curve is given by (24).

$$s(t) = \begin{cases} 0.5 * j_m \left\{ \frac{t^3}{6} + \frac{\sin\left(\frac{2\pi t}{t_j}\right)}{\left(\frac{2\pi}{t_j}\right)^3} \right\} - j_m * 0.5 * \left(\frac{t_j}{2\pi}\right)^2 t & 0 < t \leq t_j \\ -0.5 * j_m \left\{ \frac{t^3}{6} + \frac{\sin\left(\frac{2\pi t}{t_j}\right)}{\left(\frac{2\pi}{t_j}\right)^3} \right\} + j_m * 0.5 * \left(\frac{t_j}{2\pi}\right)^2 t + j_m * 0.25 * t_j^2 t + j_m * 0.25 * t_j t^2 + j_m * \left(\frac{1}{12}\right) * t_j^3 - \left(\frac{j_m}{2}\right) * t_j \left(\frac{t_j}{2\pi}\right)^2 & t_j < t \leq 2t_j \\ -0.5 * j_m \left\{ \frac{t^3}{6} + \frac{\sin\left(\frac{2\pi t}{t_j}\right)}{\left(\frac{2\pi}{t_j}\right)^3} \right\} + j_m * 0.5 * t_j^2 t + \left(\frac{j_m}{2}\right) * t \left(\frac{t_j}{2\pi}\right)^2 + j_m * 0.5 * t_j^3 & 2t_j < t \leq 3t_j \\ j_m * 0.5 * \left\{ \frac{t^3}{6} + \frac{\sin\left(\frac{2\pi t}{t_j}\right)}{\left(\frac{2\pi}{t_j}\right)^3} \right\} - j_m * 0.25 * t_j t^2 + j_m * 0.25 * t_j^2 t - \left(\frac{j_m}{2}\right) * t * \left(\frac{t_j}{2\pi}\right)^2 + j_m * \left(\frac{1}{12}\right) * t_j^3 + \left(\frac{j_m}{2}\right) * t_j \left(\frac{t_j}{2\pi}\right)^2 & 3t_j < t \leq 4t_j \end{cases} \quad (24)$$

4. RESULTS AND DISCUSSION

The position of two link robotic arm from start point to end point is shown in Table 2. It is assumed that end-effector velocity along x-direction is 20 mm/sec. Bang-bang motion produces finite acceleration at starting and ending, which makes the motion jerkiness. On the contrary, cubic polynomial produces finite jerk as shown in Table 3. The jerk-limited motion profile gives maximum velocity than other motion profiles for the given jerk (j) and motion time (t_f). However, quintic polynomial produces the lowest velocity and acceleration. The maximum velocity and acceleration produced by S-curve is lower than the other motion profile. The comparison of different motion parameters is given in Table 3.

The motion of x-coordinate of end-effector is shown in Figure 7. Figure 8 represents the motion of y-coordinate. The total time for both coordinates is the same. For fixed time, the maximum jerk magnitude along x-coordinate differs from the y-coordinate due to variation in displacement in the x and y coordinates.

Table 2. End-effector displacement at the start and end point

End-effector displacement	Initial point (mm)	End point (mm)	Kinematics constraints
x	209.3	225.4	End-effector velocity along x-direction= 20 (mm/sec)
y	250.9	223.1	

Table 3. Comparison of different motion parameters for the given time

Type of Interpolation	Total distance (mm)	J (mm/s ³)	a (mm/s ²)	v (mm/sec)	t (s)
Bang-bang motion	Δs	∞	a_m	$\sqrt{a_m \Delta s}$	t_f
Cubic polynomial	Δs	j_{m1}	$1.15 \left(\sqrt[3]{j_{m1}^2 \Delta s} \right)$	$0.66 \left(\sqrt[3]{\Delta s^2 j_{m1}} \right)$	t_f
Jerk-limited motion	Δs	j_{m2}	$0.79 \left(\sqrt[3]{j_{m2}^2 \Delta s} \right)$	$0.63 \left(\sqrt[3]{\Delta s^2 j_{m2}} \right)$	t_f
Quintic polynomial	Δs	j_{m3}	$0.38 \left(\sqrt[3]{j_{m3}^2 \Delta s} \right)$	$0.48 \left(\sqrt[3]{\Delta s^2 j_{m3}} \right)$	t_f
Cycloid motion	Δs	j_{m4}	$0.54 \left(\sqrt[3]{\Delta s j_{m4}^2} \right)$	$0.59 \left(\sqrt[3]{\Delta s^2 j_{m4}} \right)$	t_f
Harmonic jerk S-curve	Δs	j_{m5}	$0.5 \left(\sqrt[3]{\Delta s j_{m5}^2} \right)$	$0.5 \left(\sqrt[3]{\Delta s^2 j_{m5}} \right)$	t_f

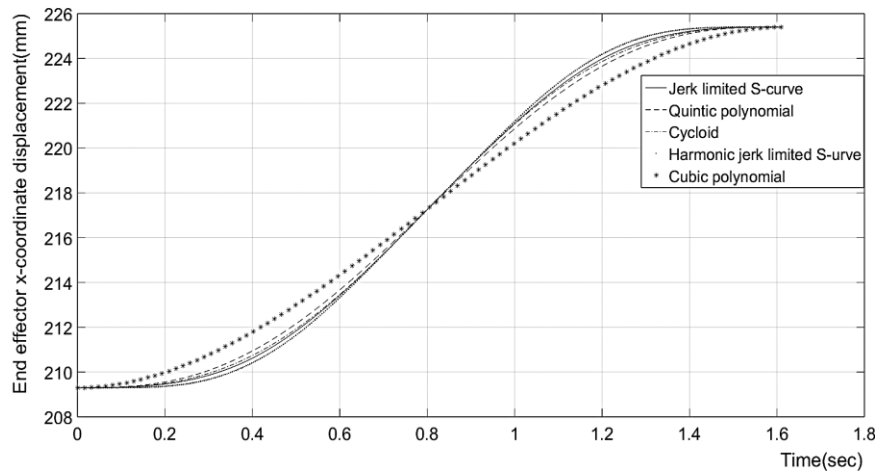


Figure 7. End-effector x-coordinate with respect to time

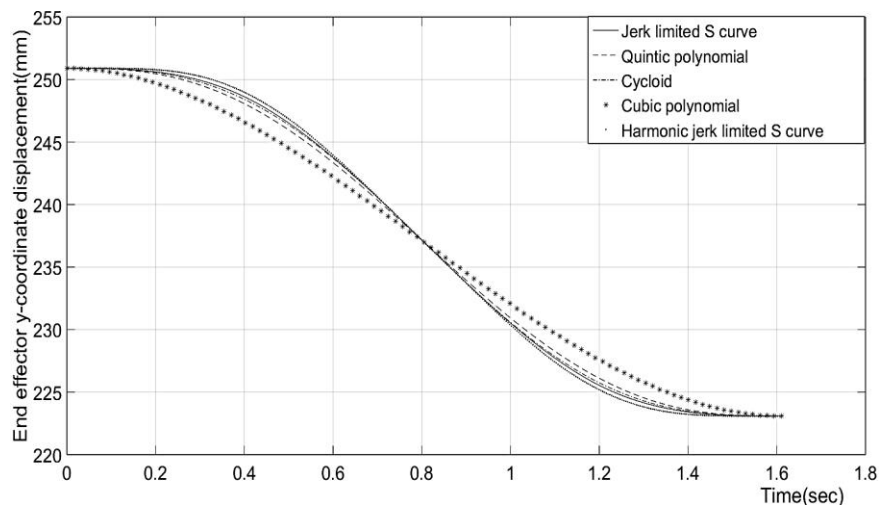


Figure 8. End-effector y-coordinate with respect to time

It can be seen that only time is synchronized, while velocity is not synchronized as shown in Figures 9 and 10. The maximum velocity of x-coordinate differs from y-coordinate velocity due to different displacement along x and y coordinates. The peak velocity of cubic polynomial is lower than the other motion profile. It can be seen that cycloid motion produces higher peak velocity than quintic motion profile. However, quintic polynomial produces the lowest peak velocity with smoothness.

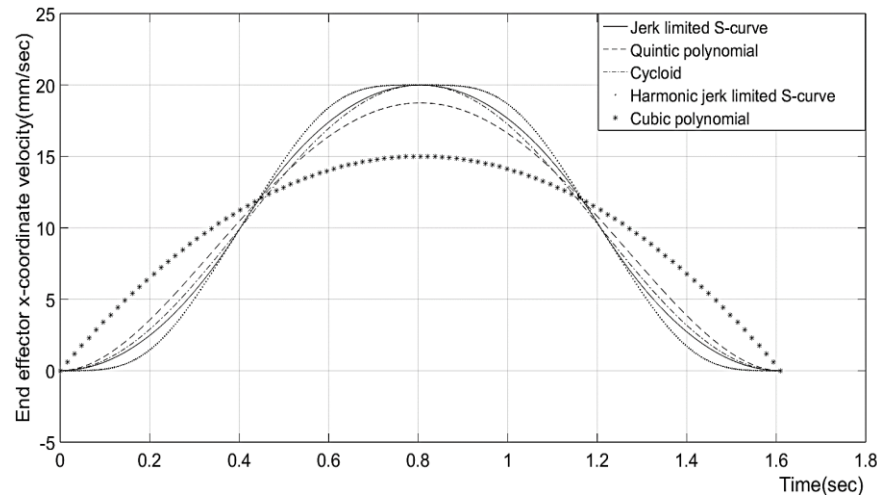


Figure 9. End-effector x-coordinate velocity with respect to time

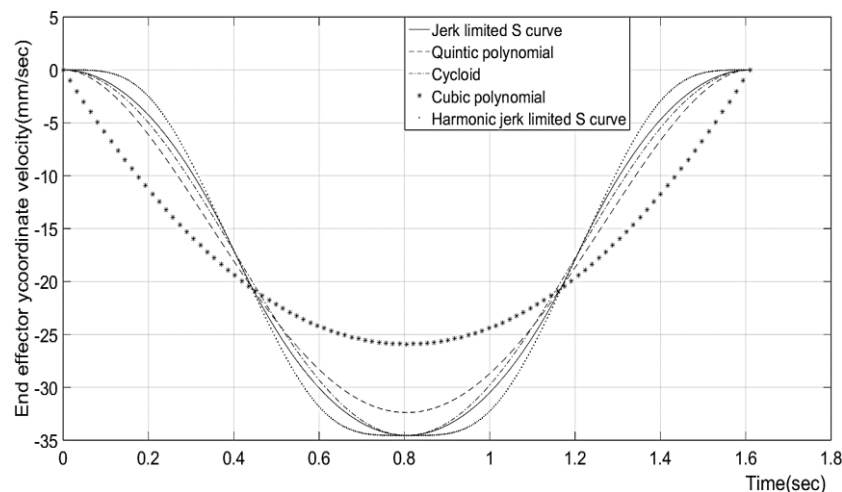


Figure 10. End-effector y-coordinate velocity with respect to time

The acceleration produced by the jerk-limited motion is not smooth. Moreover, acceleration is linear in jerk-limited motion whereas it is cubic in quintic polynomial. In contrast to cubic polynomial, acceleration of cycloid motion is zero at the starting and ending but the jerk produced by the cycloid motion is finite at the starting and ending which leads to trajectory error. The acceleration produced by the jerk-limited S-curve is linear as shown in Figures 11 and 12.

It can be seen that jerk produced by the S-curve is a step function. In quintic and cycloid motion profile jerk is continuous except at the starting and ending (finite jerk) unlike step function in jerk-limited S-curve as shown in Figure 13. The jerk magnitude of cycloid motion is higher than the jerk-limited S-curve as shown in Table 4. The maximum jerk value in the x and y direction is different due to synchronization of time as shown in Figures 13 and 14. For time synchronized motion, jerk in the x-direction is lesser than the y-direction. It was found that harmonic jerk S-curve produces maximum jerk for the given motion time as shown in Table 4.

Figure 15 shows the end-effector profile of a two-link robotic arm. The end-effector coordinates are interpolated by fifth-order polynomial. The position of joint angle for the initial and final point is calculated by inverse kinematics algorithm.

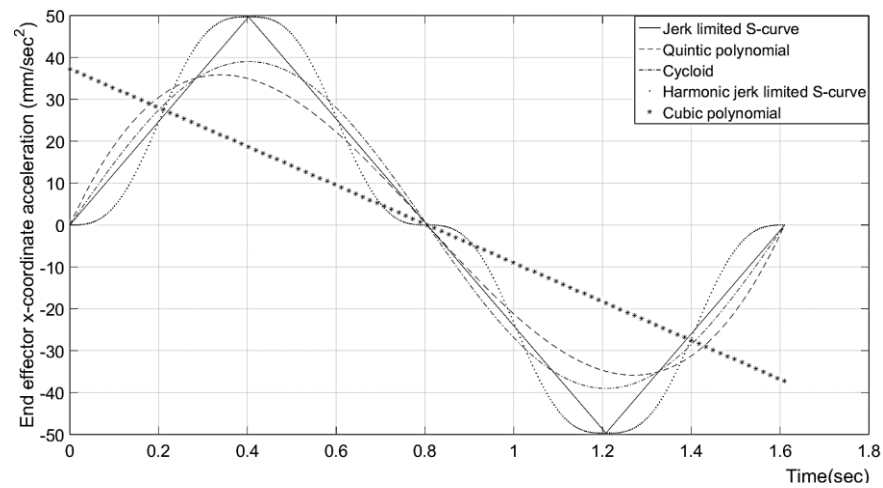


Figure 11. End-effector x-coordinate acceleration with respect to time

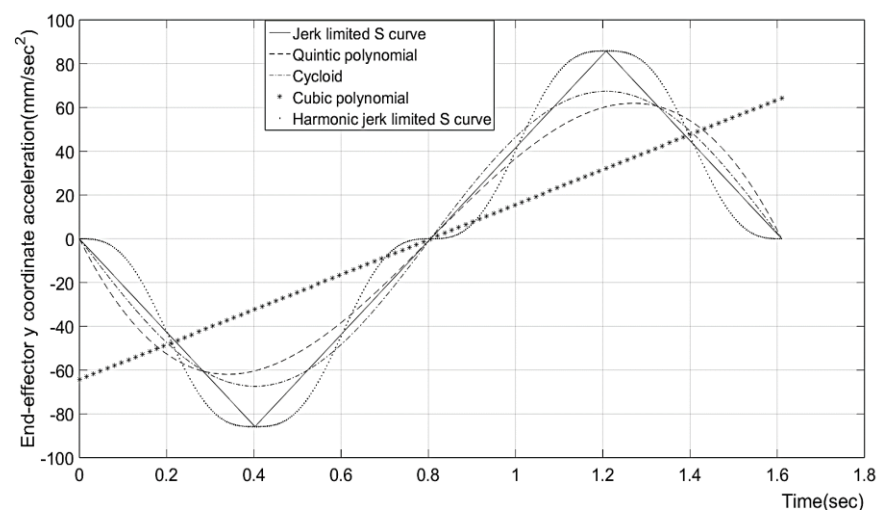


Figure 12. End-effector y-coordinate acceleration with respect to time

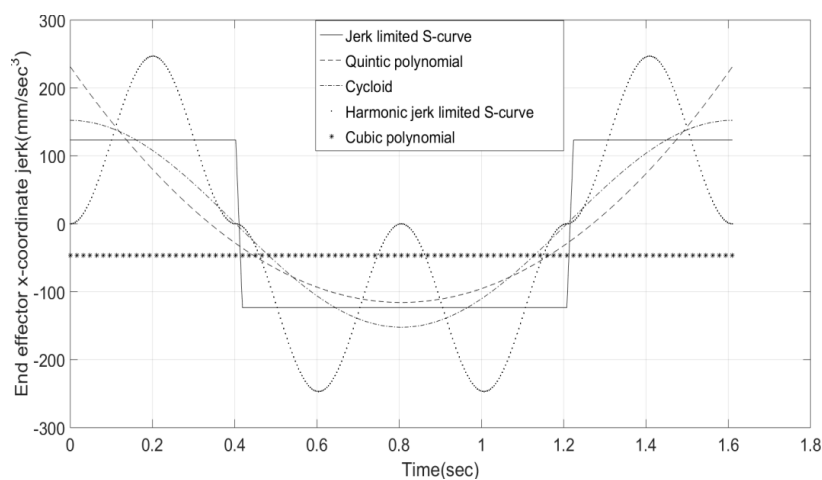


Figure 13. End-effector x-coordinate jerk with respect to time

Table 4. Comparison of jerk magnitude end-effector x-coordinate for various motion planning

Motion model	Maximum jerk value (mm/s ³)	Maximum acceleration (mm/s ²)	Maximum velocity (mm/s)
Cubic polynomial	46.3	-46.3	15
Jerk-limited S-curve	123.43	49.68	20
Harmonic jerk S-curve	246.90	49.68	20
Quintic polynomial	231.43	35.85	18.75
Cycloid motion	152.27	39.02	20

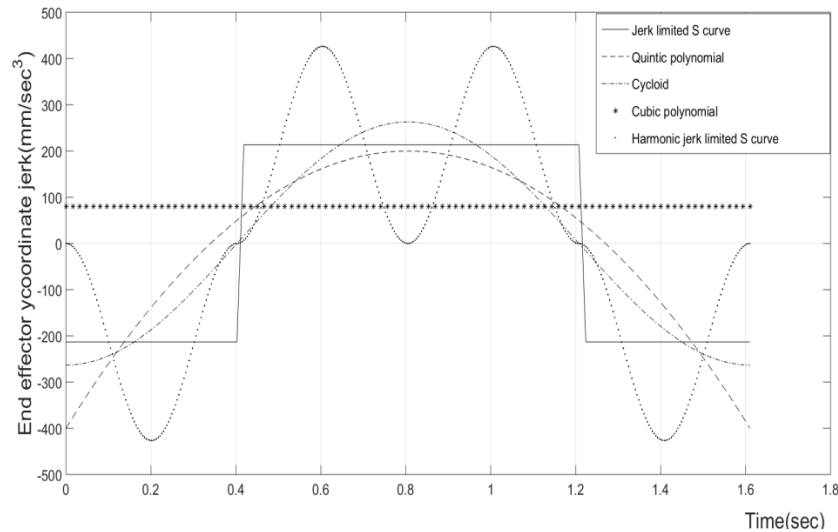


Figure 14. End-effector x-coordinate jerk with respect to time

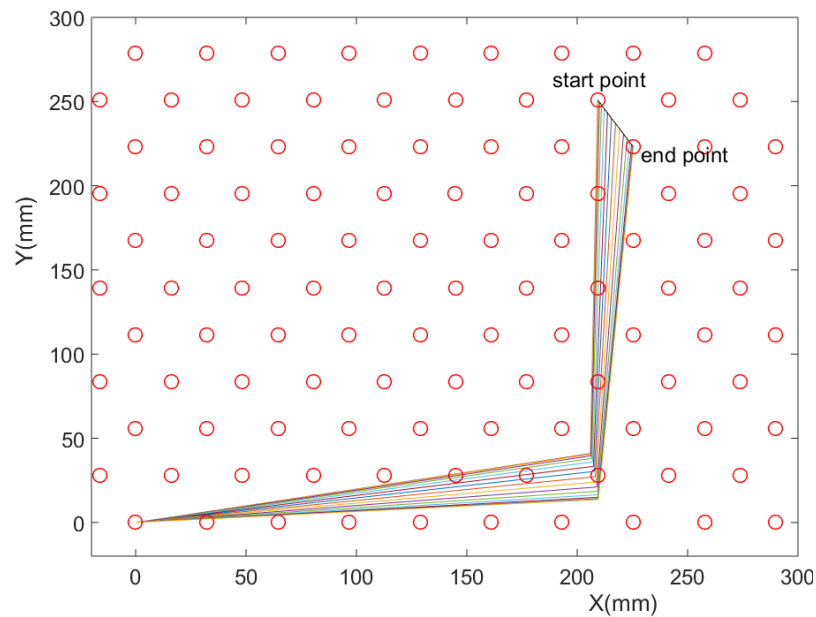


Figure 15. Two-link robotic arm end-effector profile for fifth-order polynomial

5. CONCLUSION

In this paper, the motion analysis of two-link robotic arm for steam generator inspection is discussed from kinematics aspects without considering dynamics. The theoretical formulation of fifth-order, jerk-limited and cycloid motion profile is presented, and optimal time calculation has been presented for the velocity constraints. Finally, a case study has been presented. The conclusions are summarized as follows: i) the end effector trajectory is planned by using fifth-order polynomial, cycloid motion, harmonic jerk S-curve and jerk-limited S-curve, ii) the time-optimality of motion profile considering velocity and acceleration

constraints is discussed, and iii) the synchronization of end-effector coordinates motion along the x and y direction is discussed. In future, this study can be extended to motion planning with obstacles in between the start point and end point. Moreover, comparison of various motion profiles with dynamic constraints will be studied.

ACKNOWLEDGEMENTS

Support and encouragement provided by Shri S. Raghupathy, Director, RDTG, IGCAR, and Dr. A.K. Bhaduri, Director, IGCAR are thankfully acknowledged. Perumalsamy G would like to thank Department of Atomic Energy fellowship for a perspective research grant for Ph.D.





REFERENCES

- [1] G. Perumalsamy, P. Visweswaran, J. Jose, S. Joseph Winston, and S. Murugan, "Quintic interpolation joint trajectory for the path planning of a serial two-axis robotic arm for PFBR steam generator inspection," in *Machines, Mechanism and Robotics*, 2019, pp. 637–648.
- [2] B. Ezair, T. Tassa, and Z. Shiller, "Planning high order trajectories with general initial and final conditions and asymmetric bounds," *The International Journal of Robotics Research*, vol. 33, no. 6, pp. 898–916, May 2014, doi: 10.1177/0278364913517148.
- [3] A. Kirecci and M. J. Gilmartin, "Improved trajectory planning using arbitrary power polynomials," *Proceedings of the Institution of Mechanical Engineers, Part I: Journal of Systems and Control Engineering*, vol. 208, no. 1, pp. 3–13, Feb. 1994, doi: 10.1243/PIME_PROC_1994_208_301_02.
- [4] M. Boryga and A. Graboś, "Planning of manipulator motion trajectory with higher-degree polynomials use," *Mechanism and Machine Theory*, vol. 44, no. 7, pp. 1400–1419, Jul. 2009, doi: 10.1016/j.mechmachtheory.2008.11.003.
- [5] Y. Fang, J. Hu, W. Liu, Q. Shao, J. Qi, and Y. Peng, "Smooth and time-optimal S-curve trajectory planning for automated robots and machines," *Mechanism and Machine Theory*, vol. 137, pp. 127–153, Jul. 2019, doi: 10.1016/j.mechmachtheory.2019.03.019.
- [6] M. L. Hornick and B. Ravani, "Computer-aided off-line planning and programming of robot motion," *The International Journal of Robotics Research*, vol. 4, no. 4, pp. 18–31, Jan. 1986, doi: 10.1177/027836498600400402.
- [7] Y. Fang, J. Qi, J. Hu, W. Wang, and Y. Peng, "An approach for jerk-continuous trajectory generation of robotic manipulators with kinematical constraints," *Mechanism and Machine Theory*, vol. 153, Nov. 2020, doi: 10.1016/j.mechmachtheory.2020.103957.
- [8] A. Piazzzi and A. Visioli, "Global minimum-jerk trajectory planning of robot manipulators," *IEEE Transactions on Industrial Electronics*, vol. 47, no. 1, pp. 140–149, 2000, doi: 10.1109/41.824136.
- [9] H.-I. Lin, "A fast and unified method to find a minimum-jerk robot joint trajectory using particle swarm optimization," *Journal of Intelligent & Robotic Systems*, vol. 75, no. 3–4, pp. 379–392, Sep. 2014, doi: 10.1007/s10846-013-9982-8.
- [10] F. J. Abu-Dakka, I. F. Assad, R. M. Alkhodour, and M. Abderahim, "Statistical evaluation of an evolutionary algorithm for minimum time trajectory planning problem for industrial robots," *The International Journal of Advanced Manufacturing Technology*, vol. 89, no. 1–4, pp. 389–406, Mar. 2017, doi: 10.1007/s00170-016-9050-1.
- [11] D. Constantinescu and E. A. Croft, "Smooth and time-optimal trajectory planning for industrial manipulators along specified paths," *Journal of Robotic Systems*, vol. 17, no. 5, pp. 233–249, May 2000, doi: 10.1002/(SICI)1097-4563(200005)17:5<233::AID-ROB1>3.0.CO;2-Y.
- [12] A. Piazzzi and A. Visioli, "Global minimum-time trajectory planning of mechanical manipulators using interval analysis," *International Journal of Control*, vol. 71, no. 4, pp. 631–652, Jan. 1998, doi: 10.1080/002071798221713.
- [13] G. Berselli, F. Balugani, M. Pellicciari, and M. Gadaleta, "Energy-optimal motions for servo-systems: A comparison of spline interpolants and performance indexes using a CAD-based approach," *Robotics and Computer-Integrated Manufacturing*, vol. 40, pp. 55–65, Aug. 2016, doi: 10.1016/j.rcim.2016.01.003.
- [14] P. Boscaroli and D. Richiedei, "Energy-efficient design of multipoint trajectories for Cartesian robots," *The International Journal of Advanced Manufacturing Technology*, vol. 102, no. 5–8, pp. 1853–1870, Jun. 2019, doi: 10.1007/s00170-018-03234-4.
- [15] T. Chettibi, H. E. Lehtihet, M. Haddad, and S. Hanchi, "Minimum cost trajectory planning for industrial robots," *European Journal of Mechanics - A/Solids*, vol. 23, no. 4, pp. 703–715, Jul. 2004, doi: 10.1016/j.euromechsol.2004.02.006.
- [16] M. S. Mujtaba, "Discussion of trajectory calculation methods," *Exploratory Study of Computer Integrated Assembly Systems*, California, 1977.
- [17] K. D. Nguyen, T.-C. Ng, and I.-M. Chen, "On algorithms for planning S-curve motion profiles," *International Journal of Advanced Robotic Systems*, vol. 5, no. 1, pp. 99–106, Mar. 2008, doi: 10.5772/5652.
- [18] H. Li, "A jerk-constrained asymmetric motion profile for high-speed motion stages to reduce residual vibration," *International Journal of Computer Applications in Technology*, vol. 53, no. 2, pp. 149–156, 2016, doi: 10.1504/IJCAT.2016.074453.
- [19] Keun-Ho Rew and Kyung-Soo Kim, "A closed-form solution to asymmetric motion profile allowing acceleration manipulation," *IEEE Transactions on Industrial Electronics*, vol. 57, no. 7, pp. 2499–2506, Jul. 2010, doi: 10.1109/TIE.2009.2036032.
- [20] A. Amthor, J. Werner, A. Lorenz, S. Zschaeck, and C. Ament, "Asymmetric motion profile planning for nanopositioning and nanomeasuring machines," *Proceedings of the Institution of Mechanical Engineers, Part I: Journal of Systems and Control Engineering*, vol. 224, no. 1, pp. 79–92, Feb. 2010, doi: 10.1243/09596518JSCE826.
- [21] S. Perumaal and N. Jawahar, "Synchronized trigonometric s-curve trajectory for jerk-bounded time-optimal pick and place operation," *International Journal of Robotics and Automation*, vol. 27, no. 4, pp. 385–395, 2012, doi: 10.2316/Journal.206.2012.4.206-3780.
- [22] C. DiMarco, J. C. Ziegert, and C. Vermillion, "Exponential and sigmoid-interpolated machining trajectories," *Journal of Manufacturing Systems*, vol. 37, pp. 535–541, Oct. 2015, doi: 10.1016/j.jmsy.2015.04.007.
- [23] Z. Rymanasib, P. Iravani, and M. N. Sahinkaya, "Exponential trajectory generation for point to point motions," in *2013 IEEE/ASME International Conference on Advanced Intelligent Mechatronics*, Jul. 2013, pp. 906–911, doi: 10.1109/AIM.2013.6584209.
- [24] P. A. S. Da Rocha, W. D. De Oliveira, and M. E. De Lima Tostes, "An embedded system-based snap constrained trajectory planning method for 3D motion systems," *IEEE Access*, vol. 7, pp. 125188–125204, 2019, doi: 10.1109/ACCESS.2019.2939116.





- [25] D. Simon and C. Isik, "Optimal trigonometric robot joint trajectories," *Robotica*, vol. 9, no. 4, pp. 379–386, Dec. 1991, doi: 10.1017/S0263574700000552.
- [26] A. Visioli, "Trajectory planning of robot manipulators by using algebraic and trigonometric splines," *Robotica*, vol. 18, no. 6, pp. 611–631, Nov. 2000, doi: 10.1017/S0263574700002721.
- [27] B. O. Nnaji and D. K. Asano, "Evaluation of trajectories for different classes of robots," *Robotics and Computer-Integrated Manufacturing*, vol. 6, no. 1, pp. 25–35, Jan. 1989, doi: 10.1016/0736-5845(89)90082-3.
- [28] L. Biagiotti and C. Melchiorri, "Trajectory generation via FIR filters: A procedure for time-optimization under kinematic and frequency constraints," *Control Engineering Practice*, vol. 87, pp. 43–58, Jun. 2019, doi: 10.1016/j.conengprac.2019.03.017.
- [29] S. Chand and K. L. Doty, "On-line polynomial trajectories for robot manipulators," *The International Journal of Robotics Research*, vol. 4, no. 2, pp. 38–48, Jun. 1985, doi: 10.1177/027836498500400204.
- [30] S. A. Bazaz and B. Tondur, "Minimum time on-line joint trajectory generator based on low order spline method for industrial manipulators," *Robotics and Autonomous Systems*, vol. 29, no. 4, pp. 257–268, Dec. 1999, doi: 10.1016/S0921-8890(99)00058-5.

BIOGRAPHIES OF AUTHORS







G Perumalsamy     obtained his M.Des. in Mechanical Systems in IIITDM, Kancheepuram. He is currently pursuing his doctoral degree in Engineering Science at HBNI, Mumbai, India. His thesis focuses on smooth trajectory profile generation for steam generator inspection in nuclear reactor. E-mail: perumalsamy2012mdes@gmail.com.







P Visweswaran     has been working as Scientific Officer at Indira Gandhi Centre for Atomic Research (IGCAR), Kalpakkam, India. His areas of interest are remote handling and robotic development. E-mail: visweswaran@igcar.gov.in.







Deepak Kumar     has been working at IGCAR, Kalpakkam, India since 2017. His areas of interest are remote handling and robotic development. E-mail: deepakk@igcar.gov.in.



S. Joseph Winston     has been working as Scientific Officer and The Head Remote Handling and Irradiation Experiments Division of Indira Gandhi Centre for Atomic Research (IGCAR), Kalpakkam, India. His areas of interest are in the development of remote inspection systems. E-mail: winston@igcar.gov.in.



S. Murugan     was with Reactor Design and Technology Group of IGCAR. His areas of interest are irradiation experiments, numerical modeling in welding, residual stress analysis, precision machining and fabrication, robotics and remote tooling, in-service inspection, and fast reactor engineering development. E-mail: sankmurugan1@gmail.com.